First-order Néel to columnar valence bond solid transition in a model square-lattice $S = 1$ antiferromagnet

Julia Wildeboer,[1] Nisheeta Desai,[1] Jonathan D'Emidio,[2] and Ribhu K. Kaul[1]
[1]*Department of Physics and Astronomy, University of Kentucky, Lexington, Kentucky 40506-0055, USA*
[2]*Institute of Physics, École Polytechnique Fédérale de Lausanne (EPFL), CH-1015 Lausanne, Switzerland*

(Received 5 September 2019; revised manuscript received 2 December 2019; published 13 January 2020)

We study the Néel to fourfold columnar valence bond solid (cVBS) quantum phase transition in a sign-free $S = 1$ square-lattice model. This is the same kind of transition that for $S = 1/2$ has been argued to realize the prototypical deconfined critical point. Extensive numerical simulations of the square-lattice $S = 1/2$ Néel-VBS transition have found consistency with the deconfined critical point scenario with no direct evidence for first-order behavior. In contrast to the $S = 1/2$ case, in our quantum Monte Carlo simulations for the $S = 1$ model, we present unambiguous evidence for a direct conventional first-order quantum phase transition. Classic signs of a first-order transition demonstrating coexistence including double-peaked histograms and switching behavior are observed. The sharp contrast from the $S = 1/2$ case is remarkable; we hypothesize that this is a striking demonstration of the role of the size of the quantum spin in the phase diagram of two-dimensional lattice models.

DOI: 10.1103/PhysRevB.101.045111

I. INTRODUCTION

The destruction of Néel order by quantum fluctuations is a hotly studied issue in quantum magnetism inspired originally by the parent compounds of cuprate high-temperature superconductors. In the cuprates, the Néel order appears for $S = 1/2$ moments on the square lattice. In this case, many theoretical arguments and extensive unbiased numerical calculations have put forth evidence for a fourfold-degenerate columnar valence bond solid (cVBS) phase upon the destruction of Néel order, possibly separated by the novel deconfined critical point [1–5]. More recently, inspired by the iron pnictide superconductors, a number of studies of the destruction of Néel order in $S = 1$ square-lattice systems have appeared [6–9], building on previous studies of the phase diagram of square-lattice $S = 1$ systems (see [10–14] and references therein). It is thus interesting to extend the success of unbiased quantum Monte Carlo (QMC) studies of the destruction of Néel order in square-lattice $S = 1/2$ systems [15] to the $S = 1$ case. In previous QMC studies the phase transitions in coupled $S = 1$ chains [13] and the transition to the Haldane nematic have been considered [16]. Here we will study the transition between the Néel state and a cVBS. A cartoon wave function for such a cVBS can be simply written down since two $S = 1$ spins can form a singlet from the elementary rules of the addition of angular momentum; these singlets can then be arranged in the standard columnar pattern.

The role of the microscopic value of spin on the phase diagrams of one-dimensional spin chains is now well established. Most famously Heisenberg models with integer spins realize a ground state with a gap to all excitations called the Haldane gap, whereas half-integer spin chains realize an interesting gapless ground state described at long distances by the $SU(2)_1$ Wess-Zumino-Witten field theory [17]. It is interesting to ask what the role of the size of the spin is in two dimensions. While the square-lattice Heisenberg model is Néel ordered for all spin-S, the nature of the accessible nonmagnetic phases and the theory of critical phenomena at the destruction of Néel order has been argued to depend sensitively on the value of the spin [1]. Since the subtle quantum effects that arise from Berry phase terms depend crucially on the microscopic value of the spin [18], one can expect striking differences between $S = 1/2$ and $S = 1$ even for phase transitions that appear identical with respect to the Landau-Ginzburg-Wilson criteria of dimensionality, symmetry, and order parameters. We will study this interesting issue here by focusing on the square-lattice Néel-cVBS phase transition in $S = 1$ magnets. The identical phase transition for $S = 1/2$ is described by deconfined criticality which has argued for a single continuous phase transition.

We note that a field-theoretical study has taken up a related issue previously [19]. Extending their results in a straightforward manner would suggest that a $S = 1$ Néel-cVBS transition could possibly be described by an anisotropic CP^2 field theory with quadrupled monopoles. That this implies that a *continuous* deconfined transition in our microscopic model requires a litany of additional assumptions, including that the field theory has an anisotropic fixed point, quadrupled monopoles are irrelevant at this fixed point, and that our microscopic model crosses the critical surface so we can flow into the fixed point. As we shall see below in our microscopic model we find a first-order transition, but it is unclear yet which of these assumptions fails. Further work on both microscopic models and field theory could shed light on this subtle detail in the future.

II. MODEL

Our first goal is to design a $S = 1$ sign-free model in which the Néel-cVBS transition can be studied using Monte Carlo simulations. We start with the square-lattice $S = 1$ Heisenberg

model,

$$H_J = J \sum_{\langle ij \rangle} \vec{S}_i \cdot \vec{S}_j. \quad (1)$$

This model is well known to be Néel ordered. Because we are working with $S = 1$, it is possible to square the bilinear operator and obtain an independent "biquadratic operator," $(\vec{S}_i \cdot \vec{S}_j)^2$, also amenable to QMC [20,21]. Using this term we can construct a Sandvik-like four-spin interaction [4],

$$H_{Q_K} = -Q_K \sum_{ijkl \in \square} [(\vec{S}_i \cdot \vec{S}_j)^2 - 1][(\vec{S}_k \cdot \vec{S}_l)^2 - 1]. \quad (2)$$

The sum is over all elementary plaquettes with the sites $ijkl$ being corners of the plaquettes and over both pairing assignments of ij and kl, so that the interaction preserves the square-lattice rotational symmetry, precisely as was done in the original JQ model, Ref. [4]. We note that H_{Q_K} has a higher staggered SU(3) symmetry because it is constructed from the biquadratic interaction, of which the physical SU(2) is a subgroup. However the model we study here, $H_{JQ_K} = H_J + H_{Q_K}$, has only the generic SU(2) symmetry obtained by rotating the $\vec{S}$ vector in the usual way. Previous numerical studies have established that H_{Q_K} on the square lattice has fourfold columnar VBS order [22–24]. Thus the single tuning parameter in H_{JQ_K} gives us unbiased numerical access to the Néel-VBS transition in a $S = 1$ system, as desired. We note here that H_{Q_K} is not the straightforward $S = 1$ extension of the JQ model [4]. Such a direct generalization is defined by Eq. (A12), and its study is presented in Appendix A 4: for $S = 1$ we find that the simple JQ model is always Néel ordered, no matter how large the four-spin interaction is. Therefore in contrast to the $S = 1/2$ case, the $S = 1$ JQ model does not allow us to access the quantum phase transition between Néel and VBS phases. This is why we have considered the modified interaction of Eq. (2).

Since our model is constructed to be Marshall sign positive, it can be simulated without a sign problem using the stochastic series expansion method (SSE) [25]. We have used two different algorithms as described in Appendix A 1 which produce the same results within errors. Our simulations are carried out on $L \times L$ square lattices at an inverse temperature β; all the data presented here have been checked to be in the $T = 0$ limit as shown in Appendix A 3. We work in units in which $J = 1$, and define the tuning parameter $g \equiv Q_K/J$ to access the phase transition. We study the Fourier transform of the Néel and VBS correlation functions, $S^N_{\mathbf{k}} = \frac{1}{L^2} \sum_r e^{i\mathbf{k}\cdot\mathbf{r}} \langle S^z(\mathbf{r}) S^z(\mathbf{0}) \rangle$ and $S^V_{\mathbf{k}} = \frac{1}{L^2} \sum_r e^{i\mathbf{k}\cdot\mathbf{r}} \langle S(\mathbf{r}) \cdot \mathbf{S}(\mathbf{r} + \hat{\mathbf{x}}) \mathbf{S}(\mathbf{0}) \cdot \mathbf{S}(\mathbf{0} + \hat{\mathbf{x}}) \rangle$. We define the order parameters as $\mathcal{O}^2_N = S^N_{(\pi,\pi)}$ and $\mathcal{O}^2_V = S^V_{(\pi,\mathbf{0})}$. For each of the order parameters we define ratios $R = 1 - \frac{S_{\mathbf{K}+\frac{2\pi}{L}\mathbf{y}}}{S_{\mathbf{K}}}$ (with $\mathbf{K}$ the ordering momentum); R goes to 1 in a phase with long-range order and 0 in a disordered phase. In the SSE method we map the quantum partition function of our model to a classical loop model in one higher dimension [25]. The winding number of these loops is also a useful quantity to detect the magnetic phase. The spin stiffness defined as Eq. (A9) is related to the square of the winding number of these loops, $\langle \mathcal{W}^2 \rangle$, as shown in Eq. (A10). The magnetic phase is characterized by long loops with $\langle \mathcal{W}^2 \rangle$ diverging linearly from L while the VBS phase has short loops with $\langle \mathcal{W}^2 \rangle$ going to zero.

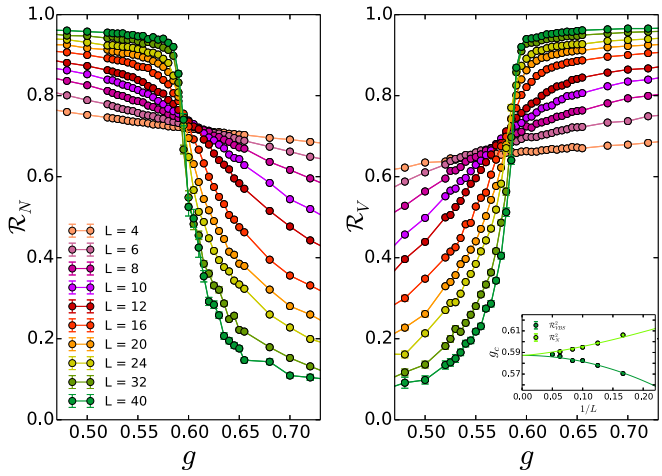

FIG. 1. Néel and VBS order parameter ratios $\mathcal{R}_N$ and $\mathcal{R}_V$ close to the quantum phase transition showing clear evidence of a direct transition. Inset shows the value of g_c obtained by analyzing crossings of L and $2L$ values for both ratios. Solid lines are a fit to the data giving $g_c = 0.588(2)$.

III. NUMERICAL RESULTS

Figure 1 shows the ratios R for the Néel and VBS order parameters as a function of g for different L. The data (see inset for finite-size scaling) provide strong evidence that the Néel-VBS transition is direct with a $g_c = 0.588(2)$; we can safely rule out coexistence or an intermediate phase. We note that this study does not by itself indicate whether the transition is first order or continuous.

The ratio data leave open the possibility of a direct continuous transition. The first indication that this does not occur is shown in Fig. 2. In this finite-size scaling plot of both order parameters, we have reasonable evidence that at the transition both order parameters are *finite*. We have carried out extrapolations on system sizes up to $L = 32$. While it is not fully reliable quantitatively to extrapolate the order parameter data with such a limited system size range, there is little doubt that both Néel and cVBS order parameters are finite at $g = 0.587$. This would indicate a first-order transition or a coexistence between Néel and cVBS phases. At a continuous transition one would expect to see the order parameters to vanish at the critical point.

Beyond system sizes of $L \approx 32$, it is very difficult to get QMC data with small error bars close to the transition point. As we now elaborate, the reason for this is that we are encountering a first-order Néel-cVBS transition. Many of the issues we encounter are similar to a previous study of a first-order Néel-VBS transition, in which the difficulties obtaining data on larger lattices are nicely explained [26]. Figure 3 shows histograms for the Néel and cVBS order parameter estimators which show clear double-peaked behavior that gets pronounced as the system size is increased. The stiffness, which is finite in the Néel phase and goes to zero in the cVBS phase, also shows clear double-peaked behavior close to the

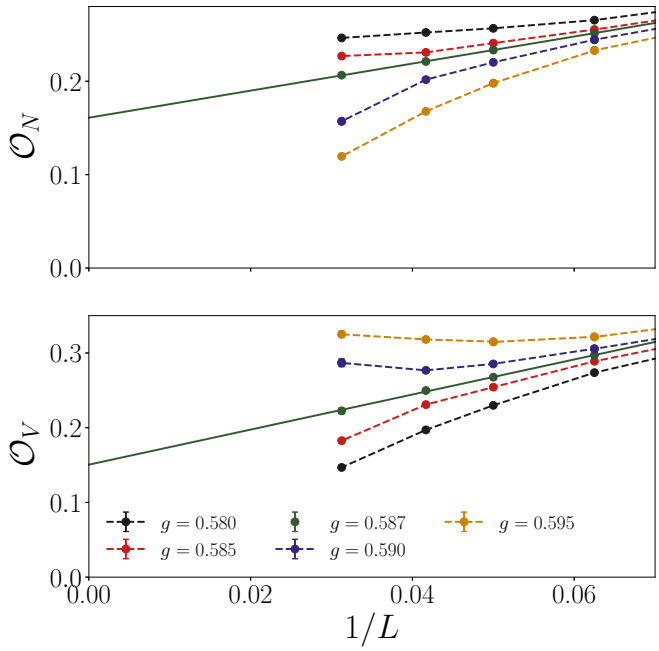

FIG. 2. Finite-size scaling of the order parameters $\mathcal{O}_N$ and $\mathcal{O}_V$ close to the phase transition on system sizes up to $L = 32$. The extrapolations to a finite value for both Néel and VBS order parameters at a common coupling $g = 0.587$ point to that fact that both order parameters are finite at the transition. The dashed lines are a guide to the eye, connecting data at the same coupling value. We have used the form $\mathcal{O}_{N,V}(L) = C_0 + \frac{C_1}{L}$ for the extrapolation. While the extrapolations are not expected to be quantitatively reliable, they clearly suggest that both order parameters are finite at the phase transition. Although this evidence is suggestive of coexistence and first-order behavior, we present extensive evidence in Figs. 3–5 that unequivocally confirms this interpretation.

transition as shown in Fig. 4. The double-peaked behavior results from the system switching between Néel and cVBS phases during the simulation. This is shown in Fig. 5 in which

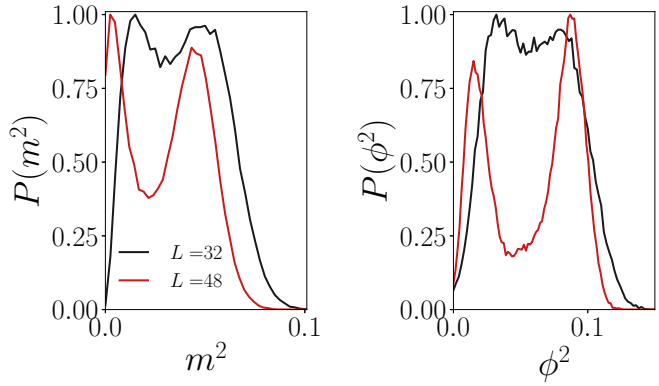

FIG. 3. Histograms of our Monte Carlo estimators m^2 and ϕ^2 that over the whole Monte Carlo run average $\mathcal{O}_N^2$ and $\mathcal{O}_V^2$, respectively. Close to the transition (at $g \approx 0.588$ and $\beta = L/4$) the probability distributions of these quantities show two peaks: One of the peaks that is close to 0 corresponds to disorder and the other one at a finite value corresponds to the ordered phase. This double-peak feature gets sharper as we increase system size, which is evidence in support of a first-order transition between the two orders.

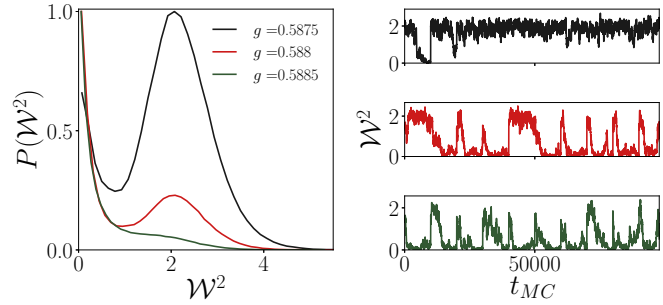

FIG. 4. Histograms (left) and Monte Carlo histories (right) of $\mathcal{W}^2$ for $L = 48$ and $\beta = 12$. Two peaks in probability distribution of $\mathcal{W}^2$ near the transition point and switching of this quantity between zero and a finite value as a function of Monte Carlo time both point to first-order behavior.

we observe clearly that when the magnetic order is present, the VBS order is absent and vice versa. This switching takes place as a function of Monte Carlo time indicating metastability, coexistence of the two orders, and hence a first-order transition. The double-peaked histogram and the switching behavior are absent in models of continuous transitions for large enough system sizes. In contrast here, these behaviors are enhanced as the system size is increased providing unequivocal evidence for a first-order transition that persists in the thermodynamic limit.

IV. CONCLUSIONS

We have introduced a model for the transition from the Néel to the fourfold-degenerate columnar valence bond solid state which is amenable to sign-free quantum Monte Carlo simulations. Previous field-theoretic work extending the $S = 1/2$ deconfined criticality scenario to $S = 1$ has argued that this transition could be direct and continuous, and described by an anisotropic CP^2 field theory. Instead, a detailed

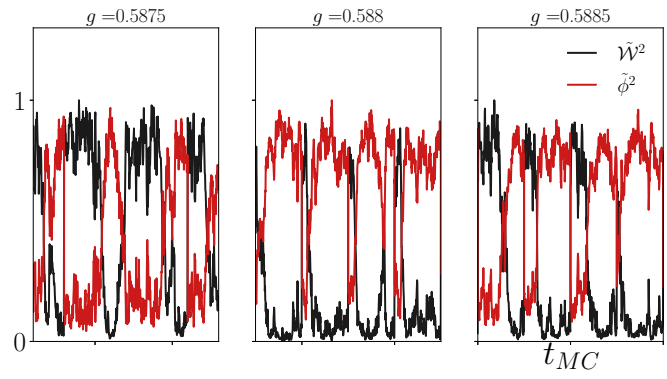

FIG. 5. MC histories of $\mathcal{W}^2$ and ϕ^2 for $L = 48$ at $\beta = 12$ show clear switching behavior in both quantities at three different couplings close to the transition point (the exact couplings are shown above each of the three figures). Here $\tilde{\mathcal{W}}^2$ and $\tilde{\phi}^2$ are normalized values of $\mathcal{W}^2$ and ϕ^2 such that the maximum is unity. It can be clearly seen that one order is present when the other is absent. We thus conclude that the system switches between the two orders at the transition point, which is characteristic of a first-order transition.

numerical study of our model shows that this phase transition is direct but of first-order in our model. With no known model that shows a continuous transition it is possible that one of the assumptions of the field-theoretic scenario is itself incorrect, e.g., the existence of an anisotropic SU(3) fixed point. Clearly more field-theoretic work is needed to further our understanding of these interesting issues. In future numerical work it will be interesting to understand how our $S = 1$ model connects to the special SU(3) point where a continuous transition has been observed in QMC simulations. Also interesting would be to understand whether the Néel-cVBS transition for $S = 3/2$ resembles the findings of the $S = 1/2$ case as expected from field-theoretic scenarios.

ACKNOWLEDGMENTS

We acknowledge partial financial support from NSF-DMR 1611161. We are grateful for the hospitality of the Aspen Center for Physics (NSF Grant No. 1607611). Computing resources were obtained through NSF XSEDE Award No. TG-DMR-140061 and the DLX computer at the University of Kentucky.

APPENDIX: NUMERICAL DETAILS

1. Algorithm

The numerical results presented in this work have been obtained using two different methods, both of which are some adaptation of the standard stochastic series expansion (SSE) [25] algorithm:

(1) In the first method we work in the $S_z = -1, 0, 1$ basis for our $S = 1$ problem. To update the SSE configurations we use both local diagonal updates and the nonlocal directed loop algorithm [27] that allows us to switch between the allowed vertices while respecting the S_z conservation.

(2) In the second method we use the split-spin representation [28,29] where each $S = 1$ is replaced by two $S = \frac{1}{2}$'s. We then simulate a $S = \frac{1}{2}$ model instead of a $S = 1$ model and project out states that only belong to the $S = 1$ subspace [16].

2. Measurements and QMC-ED comparison

We have tested our code by performing comparisons against exact diagonalization. For future reference, Tables I and II provide test comparisons between measurements obtained from a SSE study and exact diagonalization (ED) on a lattice of size $(L_x, L_y) = (4, 4)$, for various combinations of the bond and plaquette interactions J and Q_K for the J-Q_K model under investigation in this work and for various combinations of the bond and plaquette interactions J and Q_J for the spin-1 version of Sandvik's J-Q_J model (described in Appendix A 4). Due to the very large Hilbert space for this spin-1 model on a 4×4 lattice, we project out the ground state from a random state in the $S^z = 0$ subspace, thus avoiding the need to diagonalize the sparse Hamiltonian matrix. We list values for the extensive ground state energy, the Néel order parameter $\mathcal{O}_N^2$, as well as the VBS order parameter $\mathcal{O}_V^2$. Also shown are the so-called ratios $\mathcal{R}_N$ and $\mathcal{R}_V$. These quantities measured using both the algorithms described in Appendix A 1 have been checked to match. All observables are defined below.

Measurements. In order to simplify the QMC loop algorithm, we have shifted our J bond operators by the identity $J(S_i \cdot S_j - 1)$. The extensive energy quoted in the tables includes this shift. In order to characterize the Néel and the VBS phases, we measure the equal-time bond-bond correlation function $\langle S_{\vec{r}} \cdot S_{\vec{r}+\hat{\alpha}} S_{\vec{r}'} \cdot S_{\vec{r}'+\hat{\alpha}} \rangle$. Here a bond is identified by its location on the lattice $\vec{r}$ and its orientation α with $\alpha = x, y$ in two dimensions. In the VBS phase, lattice translational symmetry is broken. This gives rise to a Bragg peak in the Fourier transform of the bond-bond correlator defined as

$$\tilde{C}^{\alpha}(\vec{q}) = \frac{1}{N_{\text{site}}^2} \sum_{\vec{r},\vec{r}'} e^{i(\vec{r}-\vec{r}')\cdot\vec{q}} \langle S_{\vec{r}} \cdot S_{\vec{r}+\hat{\alpha}} S_{\vec{r}'} \cdot S_{\vec{r}'+\hat{\alpha}} \rangle. \tag{A1}$$

For a columnar VBS patterns, peaks appear at the momenta $(\pi, 0)$ and $(0, \pi)$ for x- and y-oriented bonds, respectively. Thus, the VBS order parameter is given by

$$\mathcal{O}_{VBS} = \frac{\tilde{C}^x(\pi, 0) + \tilde{C}^y(0, \pi)}{2}. \tag{A2}$$

Another useful quantity to locate a possible phase transition is the above-mentioned VBS ratio $\mathcal{R}_V$. We first distinguish between x- and y-oriented bonds:

$$\begin{aligned} \mathcal{R}_V^x &= 1 - \tilde{C}^x(\pi, 2\pi/L)/\tilde{C}^x(\pi, 0), \\ \mathcal{R}_V^y &= 1 - \tilde{C}^y(2\pi/L, \pi)/\tilde{C}^y(0, \pi). \end{aligned} \tag{A3}$$

Subsequently, we average over x and y orientations:

$$\mathcal{R}_V = \frac{\mathcal{R}_V^x + \mathcal{R}_V^y}{2}. \tag{A4}$$

This quantity goes to 1 in a phase with long-range VBS order and it approaches 0 in a phase without VBS order present.

TABLE I. The table shows the extensive energy (E), the Néel order parameter $\mathcal{O}_N^2$, and the VBS order parameter $\mathcal{O}_V^2$ obtained by exact diagonalization (ED) and by stochastic series expansion Monte Carlo (SSE) for the spin-1 J-Q_K model. Additionally shown are the ratios $\mathcal{R}_N$ and $\mathcal{R}_V$. For the SSE, errors are also shown. The MC data are computed with $\beta = 40$.

L_x	L_y	J	Q_K	E (ED)	E (MC)	$\mathcal{O}_N^2$ (ED)	$\mathcal{O}_N^2$ (MC)	$\mathcal{O}_V^2$ (ED)	$\mathcal{O}_V^2$ (MC)	$\mathcal{R}_N$ (ED)	$\mathcal{R}_N$ (MC)	$\mathcal{R}_V$ (ED)	$\mathcal{R}_V$ (MC)
4	4	0.2	0.9	−96.15381	−96.147(8)	0.13590	0.13592(2)	0.50414	0.5044(5)	0.49940	0.4993(1)	0.75713	0.7570(7)
4	4	0.5	0.2	−49.02200	−49.024(4)	0.25596	0.25594(9)	0.28370	0.2838(2)	0.78679	0.7868(1)	0.59012	0.5907(7)
4	4	0.7	0.3	−70.29052	−70.288(5)	0.24879	0.24867(8)	0.29726	0.2971(2)	0.77611	0.7760(1)	0.60493	0.6054(6)
4	4	0.8	0.4	−85.17819	−85.180(6)	0.23283	0.23291(6)	0.32728	0.3269(2)	0.75040	0.7503(1)	0.63436	0.6346(5)
4	4	0.9	0.6	−109.00470	−109.001(7)	0.20556	0.20562(3)	0.37805	0.3777(2)	0.69897	0.6989(1)	0.67619	0.6761(4)
4	4	1.0	0.59	−114.31021	−114.305(2)	0.21657	0.2168(1)	0.35766	0.35766(9)	0.72101	0.7215(3)	0.66038	0.6604(1)

TABLE II. The table shows the extensive energy (E), the Néel order parameter $\mathcal{O}_N^2$, and the VBS order parameter $\mathcal{O}_V^2$ obtained by exact diagonalization (ED) and by stochastic series expansion Monte Carlo (SSE) for the spin-1 J-Q_J (Sandvik's) model. Also shown are the ratios $\mathcal{R}_N$ and $\mathcal{R}_V$. For the MC, errors are also shown. The MC data are again computed with $\beta = 40$.

L_x	L_y	J	Q_J	E (ED)	E (MC)	$\mathcal{O}_N^2$ (ED)	$\mathcal{O}_N^2$ (MC)	$\mathcal{O}_V^2$ (ED)	$\mathcal{O}_V^2$ (MC)	$\mathcal{R}_N$ (ED)	$\mathcal{R}_N$ (MC)	$\mathcal{R}_V$ (ED)	$\mathcal{R}_V$ (MC)
4	4	0.2	0.9	−157.24324	−157.251(8)	0.33323	0.3330(1)	0.12077	0.121(1)	0.87616	0.87610(8)	0.29722	0.295(9)
4	4	0.5	0.2	−66.86936	−66.861(3)	0.34103	0.3409(2)	0.10760	0.1073(3)	0.88539	0.8854(1)	0.21940	0.215(3)
4	4	0.7	0.3	−96.79576	−96.790(5)	0.34071	0.3406(2)	0.10814	0.1079(3)	0.88501	0.8850(1)	0.22295	0.225(3)
4	4	0.8	0.4	−119.70732	−119.707(4)	0.34001	0.3402(1)	0.10935	0.1090(2)	0.88417	0.8843(1)	0.23071	0.226(3)
4	4	0.9	0.6	−158.52300	−158.520(6)	0.33873	0.3388(1)	0.11153	0.1113(3)	0.88264	0.88268(9)	0.24436	0.241(3)

The Néel structure factor is

$$m_z^2(\vec{q}) = \frac{1}{N_{\text{site}}^2} \sum_{\vec{r},\vec{r}'} e^{i(\vec{r}-\vec{r}')\cdot\vec{q}} \langle S_{\vec{r}}^z S_{\vec{r}'\alpha}^z \rangle. \tag{A5}$$

The Bragg peak appears at momentum (π, π) and thus the Néel order parameter is given by

$$\mathcal{O}_N = m_z^2(\pi, \pi). \tag{A6}$$

To additionally provide a quantity that goes to 1 in a Néel-ordered phase and vanishes in a phase without, we study the the Néel ratio:

$$\mathcal{R}_N^x = 1 - m_z^2(\pi + 2\pi/L, \pi)/m_z^2(\pi, \pi),$$
$$\mathcal{R}_N^y = 1 - m_z^2(\pi, \pi + 2\pi/L)/m_z^2(\pi, \pi). \tag{A7}$$

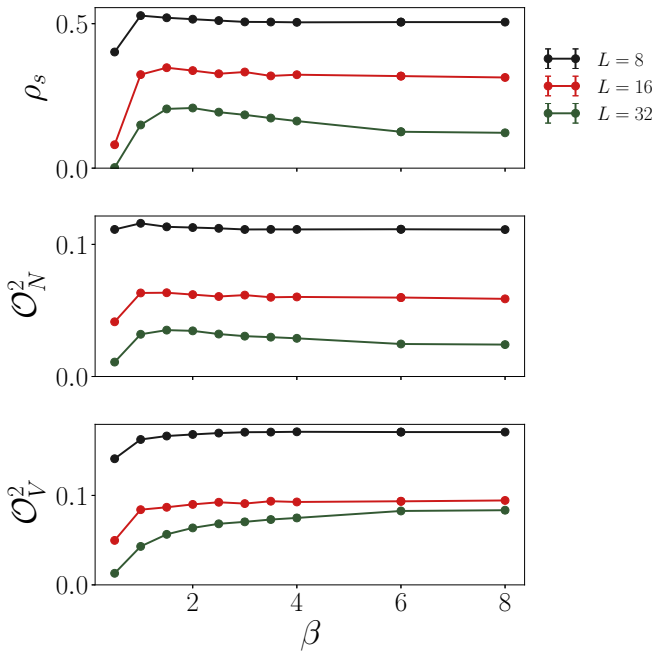

FIG. 6. Plot of observables (ρ_s, $\mathcal{O}_N^2$, $\mathcal{O}_V^2$) as a function of inverse temperature (β) shows that all observables "saturate" (changes by lowering temperature are within error bars that are on the order of 1% or smaller of quantity) as a function of β before $\beta = 8$ at $g = 0.59$. To make this more quantitative we provide the values of these observables for the biggest size presented ($L = 32$): $\rho_s(\beta = 6) = 0.126(3)$ and $\rho_s(\beta = 8) = 0.122(3)$, $\mathcal{O}_N^2(\beta = 6) = 0.0246(5)$ and $\mathcal{O}_N^2(\beta = 8) = 0.0241(4)$, $\mathcal{O}_V^2(\beta = 6) = 0.082(3)$ and $\mathcal{O}_V^2(\beta = 8) = 0.083(3)$.

We can now average over both quantities:

$$\mathcal{R}_N = \frac{\mathcal{R}_N^x + \mathcal{R}_N^y}{2}. \tag{A8}$$

The spin stiffness, ρ_s, is another quantity we use to detect the magnetic phase. It is defined as

$$\rho_s = \left. \frac{\partial^2 E(\phi)}{\partial \phi^2} \right|_{\phi=0}. \tag{A9}$$

Here $E(\phi)$ is the energy of the system when you add a twist of ϕ in the boundary condition in either the x or the y direction. In the QMC, this quantity is related to the winding number of loops in the direction that the twist has been added:

$$\rho_s = \frac{\langle \mathcal{W}^2 \rangle}{\beta}, \tag{A10}$$

where β is the inverse temperature. In the magnetic phase the stiffness extrapolates to a finite value in the thermodynamic limit, but goes to zero in the nonmagnetic phase.

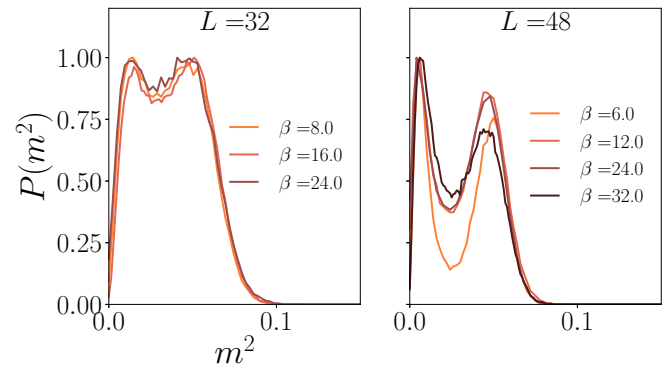

FIG. 7. Magnetization histograms for $L = 32$ (left) and $L = 48$ (right) show two peaks near the transition. The double-peak feature is not significantly weakened upon decreasing the temperature. For $L = 32$, the system shows saturation as a function of temperature; therefore the shape of the histograms does not change very much upon decreasing temperature. However, this saturation as a function of temperature is harder to see when we increase the system size to $L = 48$. This is because upon increasing the system size the tunneling barriers between the two peaks increase, making it hard to equilibrate at the transition point.

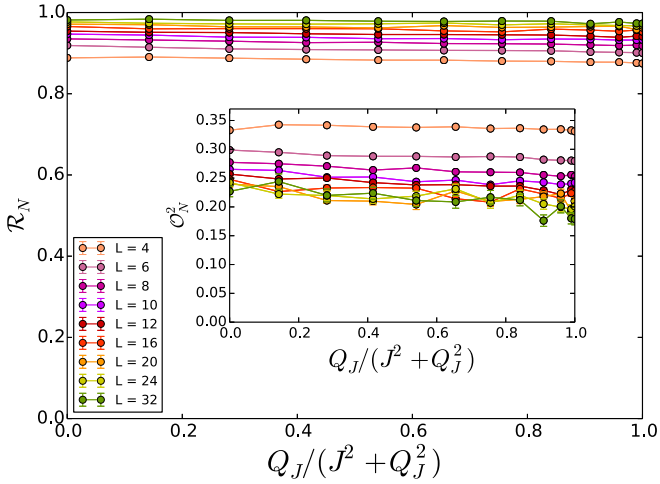

FIG. 8. Shown is the ratio $\mathcal{R}_N$ of the Néel order parameter of various values of the plaquette interaction coupling Q_J with $J^2 + Q_J^2 = 1$ for systems of size (L, L) with L up to 32 lattice sites. $\mathcal{R}_N$ appears to be independent of Q_J and approaches 1 for increasingly large system sizes indicating a phase diagram consisting entirely of Néel order. The inset shows the Néel order parameter $\mathcal{O}_N^2$.

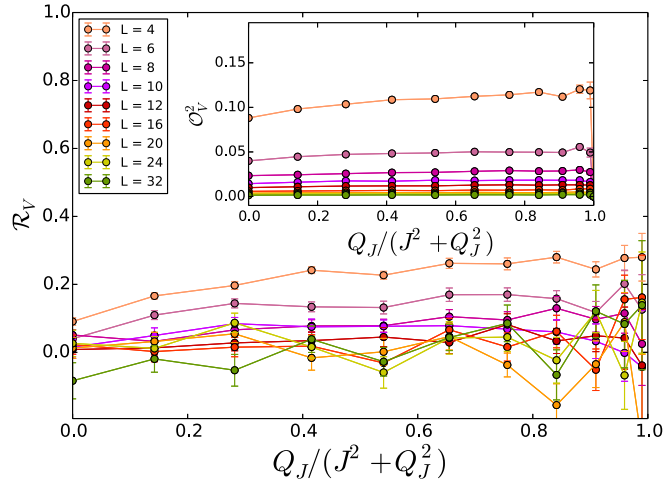

FIG. 9. Shown is the ratio $\mathcal{R}_V$ of the VBS order parameter of various values of the plaquette interaction coupling Q_J with $J^2 + Q_J^2 = 1$ for systems of size (L, L) with L up to 32 lattice sites. Confirming the findings from Fig. 8, we see that $\mathcal{R}_V$ approaches zero for sufficiently large lattice sizes independently of the coupling Q_J providing evidence for the absence of VBS order in the J-Q_J model for spin-1.

3. Ground state convergence

We investigate the behavior of the observables described above in Appendix A 2 ($\mathcal{O}_V^2$, $\mathcal{O}_N^2$, ρ_s) when the SSE is carried out at different inverse temperatures β. Figure 6 shows that these quantities saturate as a function of inverse temperature β before $\beta = 6$. However, close to the transition, one needs to go lower in temperature for saturation. Therefore we do finite-size scaling of histograms near the transition point for $\beta = L/4$ in order to probe the first-order behavior. One can see from Fig. 7 that decreasing the temperature to $\beta > L/4$ does not significantly weaken the first-order transition, so we can conclude that first-order behavior persists at zero temperature.

4. J-Q_J model for $S = 1$

We now briefly discuss another designer model Hamiltonian and compare the phase diagram for the two cases of a spin-1/2 system and a spin-1 system.

The so-called J-Q model was introduced by Sandvik in 2007 [4]. The model consists of a Heisenberg interaction between nearest-neighbor sites [see Eq. (1) in the main article] on the square lattice and an additional plaquette term:

$$H_Q = -Q \sum_{ijkl\in\square} \left(\vec{S}_i \cdot \vec{S}_j - \frac{1}{4}\right)\left(\vec{S}_k \cdot \vec{S}_l - \frac{1}{4}\right). \quad \text{(A11)}$$

The spin-1/2 case of this model $H = H_J + H_Q$ was shown to have a phase transition from Néel order to VBS order at a critical point $J/Q \approx 0.04$ [4].

We now subject the same term structure to a SSE-MC simulation in order to determine the phase diagram. We note that for the spin-1 case the constant $\frac{1}{4}$ is replaced by 1 in order by make the plaquette term amenable to the SSE-MC study:

$$H_{Q_J} = -Q_J \sum_{ijkl\in\square} (\vec{S}_i \cdot \vec{S}_j - 1)(\vec{S}_k \cdot \vec{S}_l - 1). \quad \text{(A12)}$$

The J-Q_J model spin-1 Hamiltonian is then $H_{JQ_J} = H_J + H_{Q_J}$. We analyzed the phase diagram for various couplings J and Q_J with the condition $J^2 + Q_J^2 = 1$ and found that the phase diagram consists entirely of Néel order independently of the ratio of the two coupling strengths J and Q_J. Figure 8 shows the ratio of the Néel order parameter. The ratio appears to be independent of Q_J (with J fixed by $J^2 + Q_J^2 = 1$). Further the ratio $\mathcal{R}_N$ approaches 1 for increasingly large system sizes. This is a clear indicator that the entire phase diagram consists of Néel order. For completeness we also give the ratio $\mathcal{R}_V$ of the VBS order parameter $\mathcal{O}_V^2$. In compliance with our findings from Fig. 9, we see that the ratio $\mathcal{R}_V$ approaches zero for sufficiently large lattice sizes independently of the coupling Q_J (again with J fixed by $J^2 + Q_J^2 = 1$). This provides evidence for the absence of VBS order that was present in the spin-1/2 flavor of the model.

[1] N. Read and S. Sachdev, Phys. Rev. Lett. **62**, 1694 (1989).
[2] T. Senthil, A. Vishwanath, L. Balents, S. Sachdev, and M. P. A. Fisher, Science **303**, 1490 (2004).
[3] T. Senthil, L. Balents, S. Sachdev, A. Vishwanath, and M. Fisher, Phys. Rev. B **70**, 144407 (2004).
[4] A. W. Sandvik, Phys. Rev. Lett. **98**, 227202 (2007).
[5] R. G. Melko and R. K. Kaul, Phys. Rev. Lett. **100**, 017203 (2008).
[6] F. Wang, S. A. Kivelson, and D.-H. Lee, Nat. Phys. **11**, 959 (2015).

[7] R. Yu and Q. Si, Phys. Rev. Lett. **115**, 116401 (2015).
[8] W.-J. Hu, S.-S. Gong, H.-H. Lai, H. Hu, Q. Si, and A. H. Nevidomskyy, Phys. Rev. B **100**, 165142 (2019).
[9] I. Niesen and P. Corboz, Phys. Rev. B **95**, 180404(R) (2017).
[10] T. A. Tóth, A. M. Läuchli, F. Mila, and K. Penc, Phys. Rev. B **85**, 140403(R) (2012).
[11] H. C. Jiang, F. Krüger, J. E. Moore, D. N. Sheng, J. Zaanen, and Z. Y. Weng, Phys. Rev. B **79**, 174409 (2009).
[12] J.-Y. Chen, S. Capponi, and D. Poilblanc, Phys. Rev. B **98**, 045106 (2018).
[13] K. Harada, N. Kawashima, and M. Troyer, J. Phys. Soc. Jpn. **76**, 013703 (2007).
[14] F. Michaud and F. Mila, Phys. Rev. B **88**, 094435 (2013).
[15] R. K. Kaul, R. G. Melko, and A. W. Sandvik, Annu. Rev. Condens. Matter Phys. **4**, 179 (2013).
[16] N. Desai and R. K. Kaul, Phys. Rev. Lett. **123**, 107202 (2019).
[17] I. Affleck, in *Fields, Strings, and Critical Phenomena: 49th Les Houches Summer School of Theoretical Physics* (North-Holland, New York, USA, 1990), pp. 565–640.
[18] F. D. M. Haldane, Phys. Rev. Lett. **61**, 1029 (1988).
[19] T. Grover and T. Senthil, Phys. Rev. Lett. **98**, 247202 (2007).
[20] K. Harada and N. Kawashima, Phys. Rev. B **65**, 052403 (2002).
[21] R. K. Kaul, Phys. Rev. B **86**, 104411 (2012).
[22] J. Lou, A. W. Sandvik, and N. Kawashima, Phys. Rev. B **80**, 180414(R) (2009).
[23] R. K. Kaul, Phys. Rev. B **84**, 054407 (2011).
[24] A. Banerjee, K. Damle, and F. Alet, Phys. Rev. B **83**, 235111 (2011).
[25] A. W. Sandvik, in *Lectures on the Physics of Strongly Correlated Systems XIV: Fourteenth Training Course in the Physics of Strongly Correlated Systems*, edited by A. Avella and F. Mancini, AIP Conf. Proc. No. 1297 (AIP, New York, 2010), p. 135.
[26] A. Sen and A. W. Sandvik, Phys. Rev. B **82**, 174428 (2010).
[27] O. F. Syljuåsen and A. W. Sandvik, Phys. Rev. E **66**, 046701 (2002).
[28] S. Todo and K. Kato, Phys. Rev. Lett. **87**, 047203 (2001).
[29] N. Kawashima and J. E. Gubernatis, Phys. Rev. Lett. **73**, 1295 (1994).